

Detection of Cavitation through Acoustic Generation in Centrifugal Pump Impeller

A. K. Jaiswal, A. U. Rehman, A. R. Paul[†] and A. Jain

Department of Applied Mechanics, Motilal Nehru National Institute of Technology Allahabad, Prayagraj-211004, India

[†]Corresponding author Email: arpaul@mmnit.ac.in

(Received August 4, 2018; accepted December 2, 2018)

ABSTRACT

The most common device which transport fluid in industries, agriculture as well as domestic water supply is the centrifugal pump. Based on fluid transfer conditions, several let-downs are occur in the centrifugal pump, cavitation is one among them. The flow pattern at the eye of impeller deviates from the ideal case with the occurrence of cavitation. Due to cavitation, vibration occurs on blades that generates noise in pump. In this study, the acoustics generated in centrifugal pump impeller due to cavitation is detected with the sound pressure by using 3-Dimensional, steady and unsteady state computational fluid dynamics (CFD) analysis of an industrial centrifugal pump impeller. Harmonic force analysis with blade row model helps in finding the sound pressure. The acoustics generated with unsteady-state is compared with cavitation at steady-state CFD analysis. The Reynolds averaged Navier-Stokes equations model as well as Shear Stress Transport (SST) turbulence model are used for the CFD simulation. The results show that the sound pressure calculated increases with the increase in cavitation (i.e. formation of vapour bubbles and sudden drop in head) which shows that high noises are generated by centrifugal pump impeller at lower net positive suction head (NPSH) at a particular discharge.

Keywords: Centrifugal pump impeller; Cavitation; Net positive suction head (*NPSH*); Acoustics; Sound pressure; Vapour volume fraction.

NOMENCLATURE

BEP	Best Efficiency Point	Re	reynolds number
CFD	Computational Fluid Dynamics	r	radius, m
FEM	Finite Element Method	t	blade thickness, mm
RANS	Reynolds Averaged Navier Stokes	β	Blade angle, deg
RPM	Revolution Per Minute	η	hydraulic efficiency
$NPSH$	Net positive Suction Head	σ	surface tension coefficient between liquid and vapour
$NPSH_a$	Net positive Suction Head Available	ρ	density of fluid
$NPSH_r$	Net positive Suction Head Required	ω	angular speed
SST	Shear Stress Transport		
VVF	Vapour Volume Fraction		
Symbol Description		Subscripts	
K	turbulence kinetic energy	1	inlet
M	power consumed by the pump	2	outlet
\dot{m}	mass flow rate	BEP	Best Efficiency Point
N	impeller speed	hub	hub
P	pressure	in	input
P_0	total Pressure	out	outlet
P_v	vapour Pressure	shr	shroud
Q	volume flow rate	suc	suction
R_B	radius of vapour bubble	H	hydraulic efficiency

1 INTRODUCTION

A centrifugal pump is the pressure generating hydraulic machine which transfer the electric motor or turbine energy to the kinetic energy and thereafter to the pressure energy for the fluid which is to be pumped, i.e. by providing momentum to the fluid which move from one place to other place in a system. The 3-D geometry of pump is quite complex and the internal flow is prone to strong swirl, diffusion, recirculation at inlet and exit, cavitation and flow separation with reverse flow, etc. The cavitation causes several damages to the impeller blades, shaft bearing, and performance of electric motor. due to erosion. Vibrations caused by cavitation also affects the flow passages through pipes. Cavitation is an important physical phenomenon in the process of hydraulic machines that causes many undesirable effects such as head and efficiency losses, increase in input power to pump, noise and vibration generation. A loss in pressure energy of fluid and noise generation due to adverse pressure gradient, cavitation, recirculation at inlet and outlet of the pump always occurs under off-design conditions. Thus, it becomes essential to understand the performance behaviour under off-design operating conditions.

Various authors have done experimental and numerical results studies aimed to understand and analyse the effect of flow complex mechanism in the centrifugal pump and detecting the hydraulic losses occurred in pump. [Iben \(2002\)](#) noticed that the energy equation is not required for modelling the cavitation with the fixed temperature for simulating the vapour mass fraction. [Cunha and Nova, \(2013\)](#) computationally investigated that cavitation occurrence has linear relation with the saturation (or vapour) pressure at the fixed temperature. CFD simulation helped in minimizing the cavitation phenomenon without the use of costly experimental methods. Cavitation formation increases with the increase in mass flow rate and the rotational velocity as investigated by [Muttalli *et al.* \(2014\)](#). According to [Li \(2014\)](#), the cavitation model is capable of predicting the incipient cavitation behaviour in the pump with a better accuracy and a linear constant relationship which have been found between the pump head and the integrated vapour-liquid volume ratio inside the pump impeller. Also, head becomes more and more sensitive for the integrated ratios of vapour-liquid with the increasing flow rate.

In centrifugal pump impellers, [Maxime and Chen-li \(2015\)](#) found that size of cavitation increases with the increase in blade number and rotational speed with a gradual head drop. [Mckee *et al.* \(2015\)](#) investigated industrial pump and presented different methods for detecting cavitation i.e., PCA, octave band analysis and statistical methods. They performed by dividing the data sets into three states i.e. non-cavitation, inception-cavitation, and super cavitation and they found these states by creating variance and covariance matrix for obtaining parameters datasets in a normal distribution function. In centrifugal pump impeller, the volume fraction amount got decreased with the increased outlet gauge

pressure with respect to the inlet gauge pressure ([George and Muthu, 2016](#)). [Pekker and Shneider \(2017\)](#) reported that the total head drop of the pump leads to an inter-blades flow blockage in pump impeller and at the trailing edge portion, the fluid was under higher pressure zone whereas near to the leading edge of blade, the low pressure zone occurs with the increase in number of impeller blades. Also, the flow velocity increases with the pressure drop due to inter-blade flow field which got reduced gradually and all these effects rises cavitation phenomenon.

In axial flow pump, [Shi *et al.* \(2017\)](#) investigated that tip leakage vortex (TLV) was promoted by cavitation and this can be eliminated at low cavitation. Cavitation occurrence mainly found near tip clearance, TLV and at the leading edge of the impeller blade. [Pekker and Shneider \(2017\)](#) found that inception theory was given by Zel'dovich-Fisher nucleation theory which considers the saturation of nano-voids generation and Rayleigh scattering method in detection of cavitation at the start of cavitation. [Rehman *et al.* \(2017\)](#) investigated that with the decrease in *NPSH* of the pump, the cavitation rises with the increase in vapour volume fraction on the blade surface. According to [Abdulaziz and Kotb \(2017\)](#), when pump operation shifts from non-cavitating to cavitating conditions, the vibration level increases when first blade passing frequency signs vibration spectrum with the presence of high energy at high frequency. The results revealed that using transient state analysis is capable of computing the noise produced by the pump due to cavitation.

According to result presented by [Pavesi *et al.* \(2005\)](#), the presence of jet wake pattern in the impeller passage generated an unstable vortex which further influences the flow discharge from adjacent passage and destabilizes the jet wake flow. [Dürrer and Wurm \(2006\)](#) determined overall noise level of a hydraulics and electrical drives tonal components which was related with periodical process. For constant continuous noise emission reduction in pumps, results analysis provided better vibration and noise measurements. The study by [Robinson \(2007\)](#) revealed that elimination of acoustic resonance problems in centrifugal pumps reduces shaft vibrations which results in better seal life. Also, high pressure pulsations was known to cause fatigue failures of impeller shrouds and volute tips.

[Barrio *et al.* \(2011\)](#) found that the unsteady pressure amplitude and pressure fluctuation relative magnitude influences the magnitude of flow rate pulsation and the flow rate pulsation was not changing with point of operation in the pump. [Michels *et al.* \(2012\)](#) used Expansion about Incompressible Flow technique and this separated the small acoustic fluctuations in the low pressure region of bulk flow with the some greater magnitude. In comparison with the analogy approach of acoustics, this technique extended toward the moderate Mach number (about 0.6). However, the acoustics effect and flow behaviour was resolved on several length scales of velocity.

[Al-hashmi \(2013\)](#) investigated that standard deviation (SD) and probability density function values in

centrifugal pump noise was successfully useful in detecting cavitation. According to Ferrante *et al.* (2014), integrated CFD-Acoustic approach provides cheaper, faster and highly efficient simulation chain which undertaken the traditional FEM based CFD method in acoustic design for turbofans. Mori *et al.* (2014) investigated that the acoustic pressure frequency characteristics generated in pipe flow was effecting the elastic structure vibration. Magagnato and Zhang (2015) found that the better agreements between particle image velocimetry (PIV) experiments and harmonic balance method gave unsteady results for finding the phase averaged and head and used for flow simulation which is faster for unsteady methods. Banica *et al.* (2016) found that the vane dipole source strength, blade dominating sound dipole sources, dipole at vane leading edge and rotor blade trailing edges were the functions of circumferential position.

Although several authors investigated and found the different states of cavitation in centrifugal pump impeller with varying discharge, pressure, and velocity of fluid. Also, they analysed for noise generation in centrifugal pump through experiment and the noise generated by vibration in shaft, turbulence and hydraulic losses using CFD analysis. But, limited literatures are found on the changes in sound pressure with the different states of cavitation.

The objective of the present study is to computationally determine the sound pressure at a particular value of net positive suction head (NPSH) corresponding to incipient cavitation and super-cavitation. Vapour volume fraction and drop in head in the centrifugal pump impeller are also computed with the input power and output power required for the pump. The reason for increase in harmonic sound pressure on blade is also investigated by comparing the flow pattern at different level of cavitation.

2 Numerical Formulation and Geometry

2.1 Pump Facility and Test Conditions

The pump impeller considered in this work is taken from an industrial centrifugal pump impeller (Rehman *et al.* (2015)). The impeller has three twisted backward blades with circular cross section and its geometry is modelled in CAD software 'Catia-V5' (Fig. 1). The major dimensions associated to the pump impeller are presented in Table 1.

2.2 Grid Generation

The geometry construction was followed by grid generation. This is one of the most complicated process and time consuming process in finding the suitable mesh. In solving the N-S equations through CFD, the calculation for the domain must be separated into a large number of refined cells. The Mesh was generated in Mesh modeller 'Ansys-16.0 Workbench' using tetrahedral element with setting patch independent algorithm (Rehman *et al.*, 2017) as shown in Fig. 2. The mesh qualities, boundary conditions, and discretization schemes are tabulated in Table 2.

Table 1 Main dimensions of the centrifugal pump impeller

Parameter	Dimension
Blade thickness, t	6 mm
Impeller inlet blade angle, β_1	25°
Impeller outlet blade angle, β_2	16°
Impeller inlet diameter, D_1	156 mm
Impeller outlet diameter, D_2	399 mm
No. of blades	3
Outlet blade width, B_2	22.5 mm

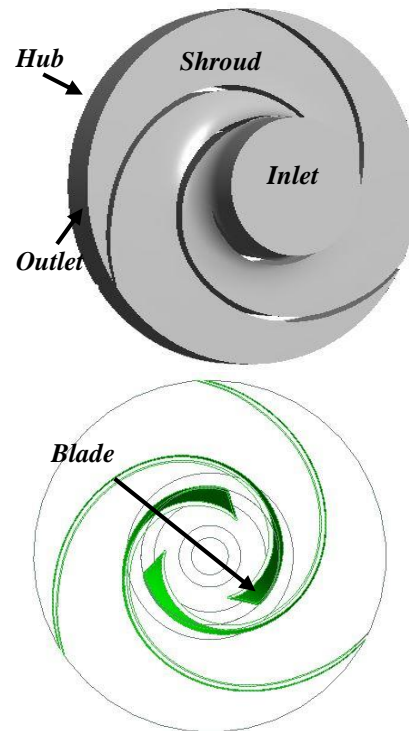


Fig. 1. Geometry model of centrifugal pump impeller.

Table 2 Meshing and boundary condition details

Parameter	Description
Flow domain	Impeller
Mesh/Nature	Unstructured
Total elements	1629393
Max. element size	3.3 mm
Max. skewness	0.87
Max. aspect ratio	12.45
Max. orthogonality	0.99
Fluid flow type	Multiphase flow
Fluids Nature	Water and Water vapour at 25°
Turbulence model	SST $k-\omega$
Inlet condition	Total pressure at Stationary frame
Outlet condition	Bulk mass flow rate
Saturation pressure	4805.256 Pa
Time step for transient	0.0034 s
Number of Revolution per period	4 revolution
Convergence value	10 ⁻⁴
Time for single simulation	6-36 hours
Iteration steps	2-3000

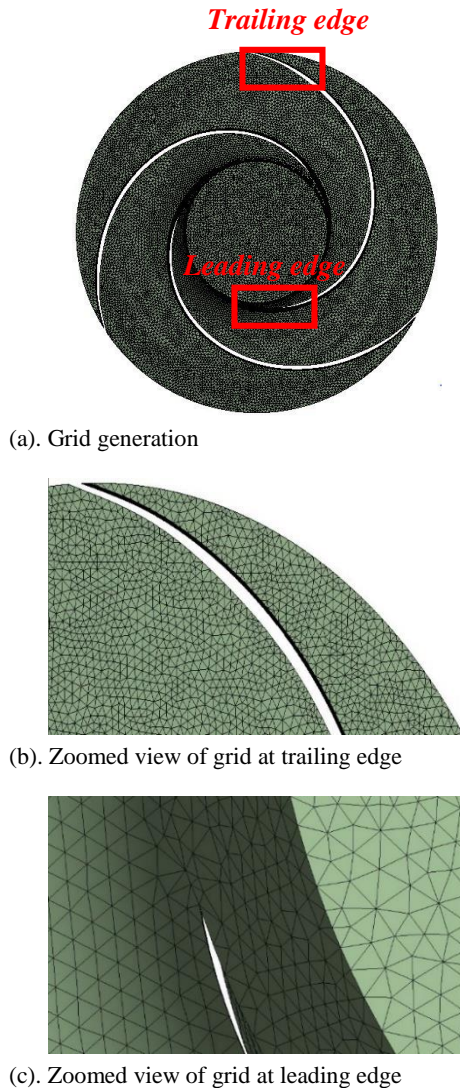


Fig. 2. Meshing of centrifugal pump impeller with leading and trailing edge.

2.3 Mathematical Modelling

2.3.1 Governing Equations

The incompressible, steady and RANS equations are used for calculating the flow parameters in a rotating impeller system of the centrifugal pump.

2.3.2 Continuity Equation

The mass conservation equation for incompressible flow is given by

$$\nabla \cdot \vec{w} = 0 \quad (1)$$

2.3.3 Momentum Equation

$$\vec{w} \cdot \nabla \vec{w} = -2\vec{\omega} * \vec{w} + \omega^2 \cdot \vec{r} - \frac{1}{\rho} \nabla \rho + \frac{1}{\rho} \nabla \cdot \tau \vec{w} \quad (2)$$

Here ' w ' is relative fluid velocity, ' ω ' is angular rotation speed of the impeller, ' r ' is radial location and ' p ', ' ρ ' are pressure and density respectively. The viscosity and the turbulent viscosity has been included by stress tensor ' τ ' $\tau_{ij} = 2\mu \cdot s_{ij} - \rho \cdot w_i \cdot w_j$. Since, ' μ ' is dynamic viscosity and ' s_{ij} ' is strain

tensor. Reynolds stress due to turbulent motion is represented in second term on the right side of above equation and the finite element volume approach has been used in discretizing the governing equations by using hybrid differencing scheme.

2.3.4 Turbulence Models

In this study, shear stress transport (SST) $k-\omega$ turbulence model is used as it allows determination of both the turbulent length scale and time scale by solving the turbulence/frequency based $k-\omega$ model at the wall and standard $k-\epsilon$ model in the bulk flow region i.e. high Reynolds number (Rehman *et al.*, 2017). Steady-state transport equations used in formulating the turbulent kinetic energy ' k ' and rate of dissipation ' ϵ '.

$$\frac{\partial}{\partial x_i} (\rho k u_i) = \frac{\partial}{\partial x_j} \left[\left(\mu + \frac{\mu_t}{\sigma_k} \right) \frac{\partial k}{\partial x_j} \right] + G_k + G_b - \rho \epsilon - Y_M + S_k \quad (3)$$

$$\frac{\partial}{\partial x_i} (\rho \epsilon u_i) = \frac{\partial}{\partial x_j} \left[\left(\mu + \frac{\mu_t}{\sigma_\epsilon} \right) \frac{\partial \epsilon}{\partial x_j} \right] + C_{1\epsilon} \frac{\epsilon}{k} (G_k + C_{3\epsilon} G_b) - C_{2\epsilon} \sigma \frac{\epsilon^2}{k} + S_\epsilon \quad (4)$$

2.4 Formulation

The pump performance parameters such as head, input power to shaft and hydraulic efficiency are calculated from the equations that are given below.

The pump head is the measurement of kinetic energy created by the centrifugal pump. Head measures the energy of the pump and is calculated by

$$H = P_2 - P_1 / \rho g \quad (5)$$

where, P_1 and P_2 are the static pressures at the inlet and outlet of the centrifugal pump respectively.

The output power by the pump is the amount of energy per unit time transformed from electric energy to potential energy neglecting other losses to the pump. The output power is basically calculated by

$$P_{out} = \rho g Q H \quad (6)$$

Then, the overall performance of the centrifugal pump was determined by considering input power and output power by the centrifugal pump and thus, the hydraulic efficiency is determined by

$$\eta_{pump} = P_{out} / P_{in} \quad (7)$$

2.5 Cavitation Model

Cavitation is the process analogous to boiling of a liquid, although it is the pressure reduction without heat addition. Cavitation occurs when the pressure falls below the vapour pressure. Cavitation causes formation of cavity in pump impeller. The degree of cavitation is estimated in terms of Net Positive Suction Head ($NPSH$), which is defined as

$$NPSH = \frac{P_{01}}{\rho g} - \frac{P_v}{\rho g} \quad (8)$$

$$R_B \frac{d^2 R_B}{dt^2} + \frac{3}{2} \left(\frac{dR_B}{dt} \right)^2 + \frac{2\sigma}{\rho R_B} = \frac{P_v - P_{0l}}{\rho} \quad (9)$$

where P_{0l} is total pressure at upstream, P_v is vapour Pressure of flowing liquid, R_B represents the bubble radius, σ is the surface tension coefficient between liquid and vapour, ρ is density of liquid and g is the acceleration due to gravity. The cavitation model is used by considering two fluids pair models i.e. water at 25°C and water vapour at 25°. Rayleigh-Plesset Eq. (9) is used for calculating time-varying cavitation bubbles of radius size 10^{-6} m (ANSYS CFX-Solver Theory Guide, 2016). Water has saturation pressure of 4805.256 Pa for converting it into the vapour form. The volume fraction of 100% and 0% are used for water and water vapour respectively. The first appearance of cavitation in the flow domain of a centrifugal pump is called 'incipient cavitation'. When the available net positive suction head ($NPSH_a$) is decreased from its inception level ($NPSH_i$), cavitation enlarges and starting to cause noise, and eventually leading to cavitation damage, performance change and head breakdown. The $NPSH$ at which the head developed by pump drops below 3% or more of its maximum head available at a given flow rate, severe cavitation occurs, which is denoted as 'super cavitation' ($NPSH_{3\%}$) which greatly affects the performance of the pump.

2.6 Boundary Conditions and Solver Settings

Total pressure at stationary frame is specified at the inlet of the pump impeller while bulk mass flow rate is specified at its outlet, assuming steady state condition for cavitation and transient state condition with simulating blade row for acoustics. An iterative upwind scheme is used with fully implicit discretization solving hydrodynamic equations for velocity and pressure as a single system in coupled form.

2.7 Transient blade Row Model

The transient, time transformation method analysis using blade row model available in Ansys-CFX occurs as a result of interaction for single blade row, blade flutter, or boundary disturbances. This model reduce the size of the computational problem (memory and computational time) by solving the blade row solution for one or two passages per row. The details used for transient condition is given in Table 2. For finding the sound pressure, the simulated results of harmonic force response on blade surface are exported at the end of passing period. Thereafter, a point is selected from the exported results at the impeller eye on blade surface. The root mean square values denote the sound pressure in terms of harmonic pressure (or sound pressure) computed on chosen point of the blades.

2.8 Grid independency and Validation

The final grid is selected through grid independency test as shown in Fig. 3. The variation in head (257.4 m) is found to be negligible after simulation with 1.63 million elements compared shown in Fig. 3, hence the grid size of 1.63 million is chosen for

further analysis. The chosen grid has a skewness of 0.87 at the mass flow rate of 67.32 kg/s and impeller speed of 2933 RPM. The generated grid corresponding to 1.63 million elements is shown in Fig. 2.

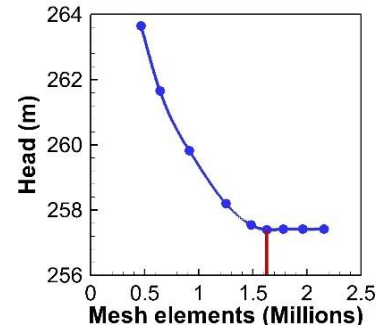


Fig. 3. Grid Independency test of meshed impeller.

The CFD results has been validated with the experimental results reported by Rehman *et al.* (2017) for water as the working fluid agreed well with efficiency deviation of 3-4.5% at the BEP of the pump as shown in Fig. 4.

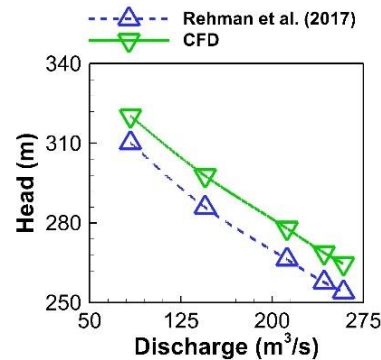


Fig. 4. Validation of CFD results.

3 RESULTS AND DISCUSSION

3.1 Performance Curve

3.1.1 Head Drop Curve for Cavitation

The head flow curve predicted the capacity of pump impeller (Pode *et al.*, 2015). The variation of head and vapour volume fraction with $NPSH$ for different mass flow rate is shown in Fig. 5. The figures shows that the head goes on decreasing after the incipient cavitation started and a drop of 3% or more is achieved at lower $NPSH$ of the pump impeller, which is denoted as 'super-cavitation'. Occurrence of cavitation can also be predicted by considering the vapour volume fraction (VVF) generated within the impeller as the $NPSH$ decreases. Figure 5 recorded 14% or more rise in VVF after occurrence of incipient cavitation in the pump impeller. The graph for different mass flow rates best suits the pattern of head drop with the rise in VVF at the particular $NPSH$.

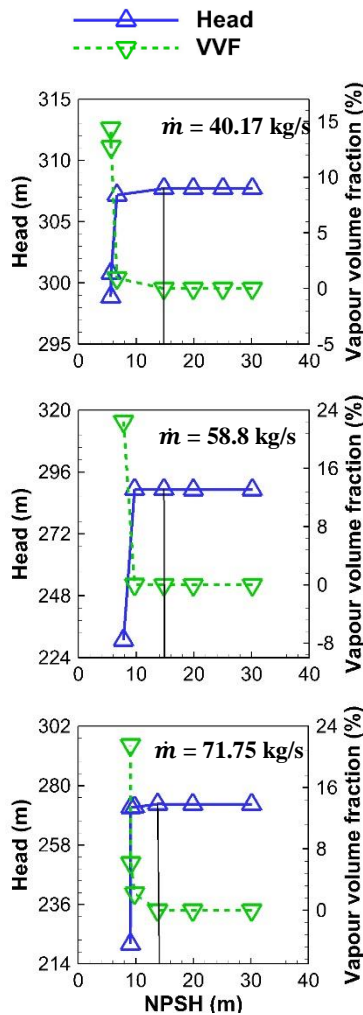


Fig. 5. Performance of head and vapour volume fraction curve due to cavitation with *NPSH* of pump impeller for different mass flow rate.

3.1.2 Power and Efficiency Variation during Cavitation Period

The input power is a function of the density, head, and flow rate; hence, the power required by pump impeller at the different stages of cavitation are analysed. Figure 6 shows the variation of input power and output power for different flow rates through the pump impeller by decreasing *NPSH*. The output power curve attains similar pattern as the head and the input power required by impeller and is decreased with lowering *NPSH* but a sudden drop of input power (5% or more) is noticed with the sudden drop of output power (3% or more). This effect is due to the decrease in inlet total pressure required by pump with *NPSH* as described in Eq. (8) Since, output power is directly proportional to head and density of water according to Eq. (2), therefore, as the head drops, output power also decreases.

3.1.3 Head and Efficiency Variation during Cavitation

In Fig. 7, the efficiency of pump impeller increases

with decrease in *NPSH* but a steady increase in efficiency curve is observed between incipient cavitation and super-cavitation and thereafter, a sudden decrease in efficiency is noticed until it reaches to super-cavitation. The increase in efficiency is because the output power obtained decreases monotonically as *NPSH* is being lowered, while the input power required decreases considerably as shown in Fig. 6. Hence, the efficiency increases steadily before the super-cavitation point. However, impeller efficiency decreases suddenly immediately before the super-cavitation point because beyond this point, small decrease in *NPSH* decreases both output power and input power, but the rate of decrease in output power is larger than input power (as discussed earlier). Thus, there is sudden drop of efficiency computed at low *NPSH*

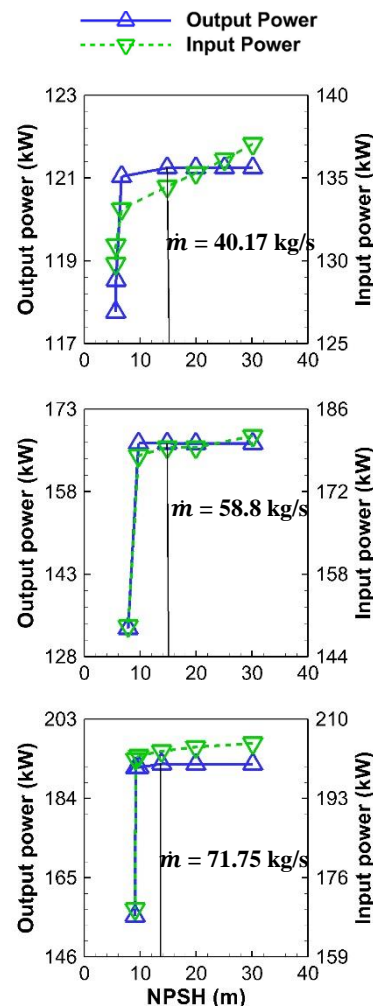


Fig. 6. Variation of output power and input power with *NPSH* of pump impeller for different mass flow rate.

3.2 Analysis of Cavitation at Different Location

3.2.1 Cavitation on Blades

It is seen from the results presented in the preceding section that as *NPSH* of pump impeller decreases, the occurrence of cavitation increases. The first

appearance of vapour bubble observed is called as incipient cavitation (Li, 2014). The appearance of this first bubble is mainly on the eye of impeller as shown in Fig. 8. Fig. 8(a) shows the presence of incipient cavitation for different mass flow rates. It represents that the incipient cavitation has only occurred on the surface of impeller blade. As the *NPSH* decreases, the formation of bubbles increases and covers the inlet portion of blades. The formation of bubbles are only at suction portion of blades because the area of blade at suction of impeller eye is very low which results in increase in fluid velocity at pump suction, as per Bernoulli's principle, higher fluid velocity means higher velocity and lower pressure head and thus making low pressure and cavitation at suction of impeller blade (Pump Cavitation Causes, 2018).

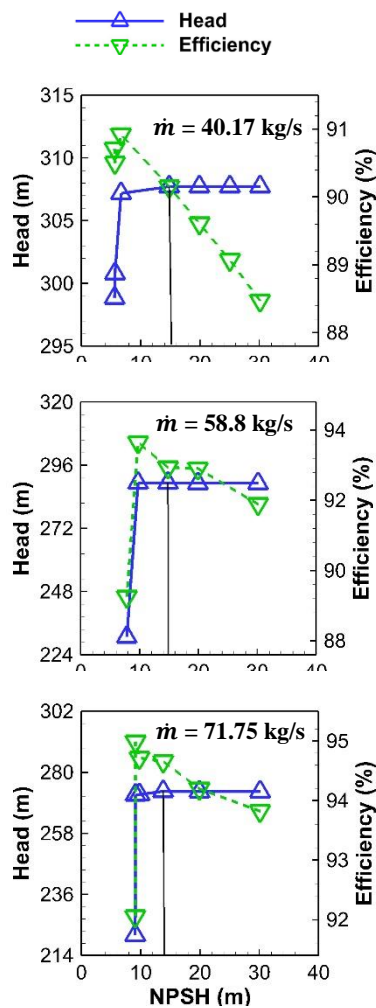


Fig. 7. Performance variation of head and efficiency with *NPSH* of pump impeller for different mass flow rate.

3.2.2 Cavitation at Suction Pipe or Impeller Inlet

The cavitation has also occurred at the suction of

the impeller. Figure 8(b) and 8(c) shows the presence of cavitation at blade and inlet of the impeller for maximum efficiency and for minimum head (i.e. super-cavitation) respectively. In Fig. 8(b), as the *NPSH* of the impeller decreases further from the incipient cavitation, the presence of cavitation from blade to the impeller inlet is found as increasing. The reason for cavitation expansion is that the pressure required by impeller for the same rotation speed decreases with the decrease in *NPSH*. The decrease in pressure decreases pressure head at the inlet of impeller that is responsible for cavitation. Figure 8 (c) shows super cavitation for different mass flow rates. In Fig. 8 (c), massive cavitation generated within the impeller compared to previous cases. This is because of drastic head drop occurred at very low *NPSH* of the pump impeller.

3.3 Sound Pressure Analysis

Various components contributed the noise emission in the pump, e.g. originating from the hydraulics, pressure pulsations and electromagnetic forces in the electrical drive, cavitation occurrence, or presence of turbulence in fluids (Dürer and Wurm, 2006). In the previous sections, it is seen that as the head decreases, the vapour volume fraction increases then huge amount of vapour bubbles are formed when these bubbles collapses then they produces noise and some pressure on blades then these pressure causes vibration in the blades and due to vibration the noise are produced by the pump. These effect is due to pressure fluctuations or pulsations and the fluid-structure interaction with rotating blades and the cutwater are considered as the main causes of water-borne noise radiating from a centrifugal pump (Al-hashmi, 2013). Additionally, cavitation produces noise generation and this mechanism is known as cavitation noise in which the bubbles collapses randomly, therefore produces turbulent acoustics. Thus, we can detect the cavitation in the centrifugal pump impeller through the acoustics produced by the impeller blades.

Figure 9 shows the variation of sound pressure and head with the occurrence of cavitation for different mass flow rates. In Fig. 9, sound pressure curves increase with the decrease of *NPSH* beyond incipient cavitation point. This is due to occurrence of super-cavitation, which makes the operation of the pump impeller noisier due to vibration. Similar relationship was found by Abdulaziz and Kotb (2017).

3.4 Flow Velocity Analysis

Figure 10. and Fig. 11 represent the velocity streamline for incipient cavitation at different mass flow rate and for different level of cavitation for a particular mass flow rate (40.17 kg/s) respectively. In Fig. 10, the velocity at incipient cavitation increases with the increase in mass flow rate from

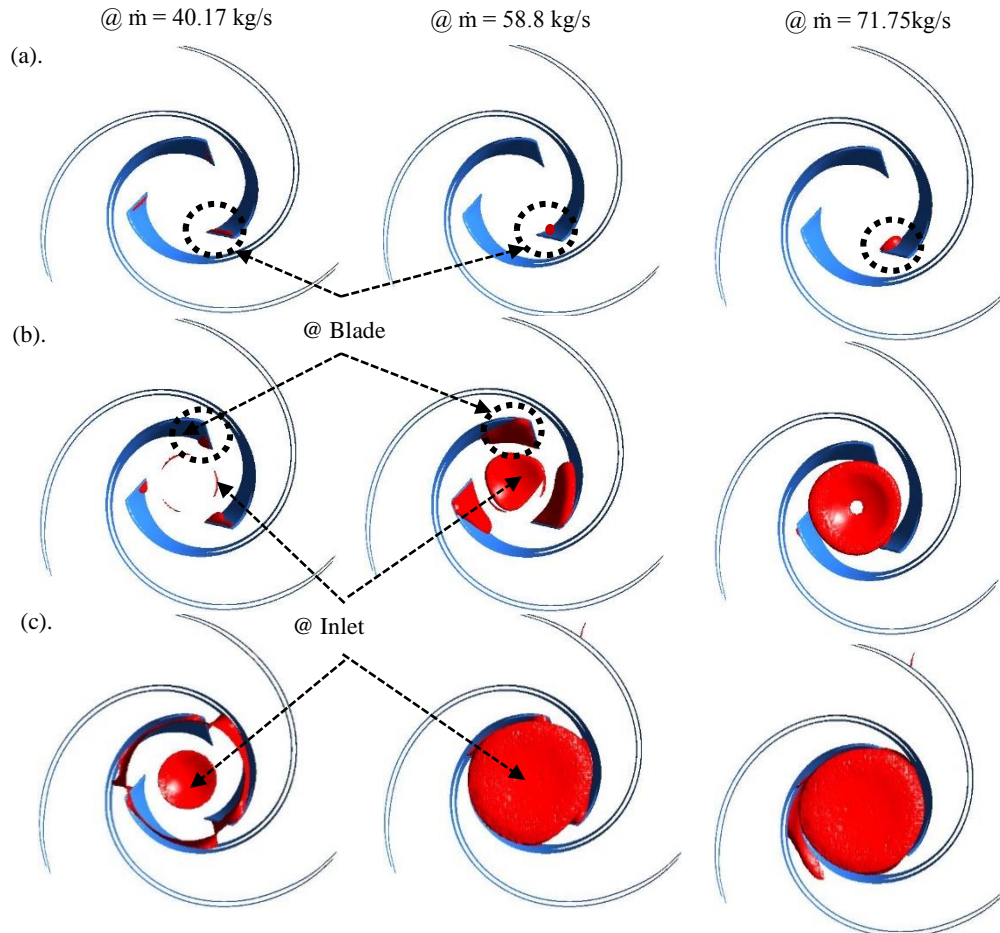


Fig. 8. Occurrence of (a). incipient cavitation (b). cavitation where efficiency is maximum and (c). super cavitation for different mass flow rate.

40.17 to 71.75 kg/s. This is because the area throughout the impeller passage is constant while mass flow rate on increase, resulting an increase of velocity through the passage (Zhou *et al.*, 2003). In Fig. 11, the velocity at a mass flow rate of 40.17 kg/s is found on increasing as the cavitation in the pump impeller changes from incipient to super cavitation.

Figure 12. shows the pressure contour of the pump impeller from incipient cavitation to super cavitation at mass flow rate of 40.17 kg/s. The pressure at inlet and outlet of the impeller goes on decreasing because the *NPSH* of the pump impeller decreases and there is rise in cavitation as the pressure throughout the pump impeller decreases (Rehman *et al.*, 2017). With the rise in pressure when vapour bubble collapses inside the pump, the vapour strikes the metal parts at the speed of sound.

The cavitation on blades surfaces is responsible for erosion of blade materials due to pitting on blade surface, also it deteriorates the blade surface and casing surface. Fig. 13 represents the wall shear stress on the blades of pump impeller due to accumulation of vapour bubbles at a mass flow rate of 40.17 kg/s. The shear stress on blades during incipient condition is found very low and

mostly dominates near the leading edge of the blades. As the cavitation level increases, the action of shear due to vapour bubbles also increases and covers almost the 40% of the blade surfaces. Bubble's furthest side from the wall, oriented inwards, towards the solid boundary and hit the wall with very high speeds enough to remove the material (Binama *et al.*, 2016). This hitting of bubbles on the blade causes shear stress generated on the surface of the blades. This would eventually cause pitting on the blade surface and subsequently material loss from it, leading to increase of surface roughness and unbalancing of impeller.

4. CONCLUSIONS

The performance of centrifugal pump impeller for both steady and unsteady conditions are analysed under all possible cavitation situations. The following conclusions are drawn from the present study.

- The efficiency of the pump impeller increases up to a certain level of *NPSH* (called incipient *NPSH*), beyond which sudden drop of output power is noticed with massive drop in impeller head.

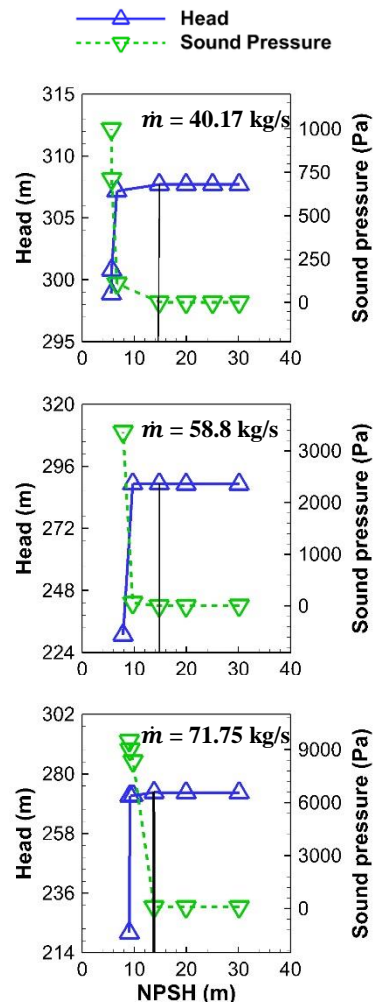


Fig. 9. Variation of sound pressure and head with *NPSH* of pump impeller for different mass flow rate.

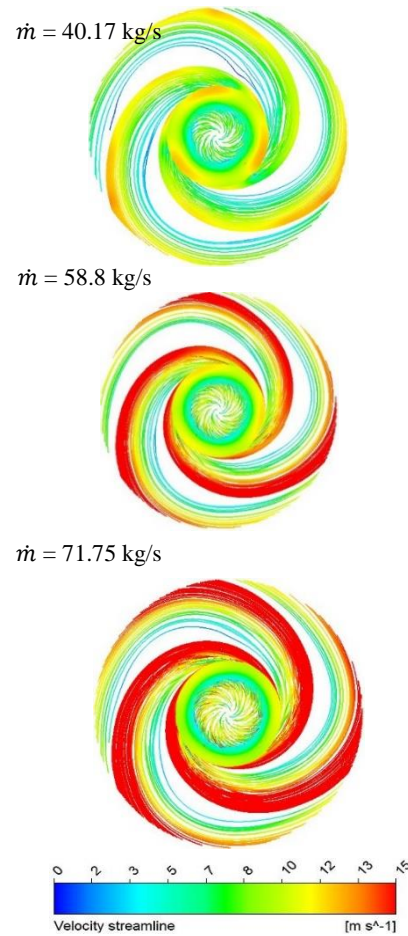


Fig. 10. Velocity streamline at incipient cavitation for

- ❖ The incipient cavitation is observed only at the tip of the impeller blade. The cavitation is however observed at the suction pipe and at inlet of the pump impeller if *NPSH* decreases further after incipient cavitation.
- ❖ The velocity is on increase while static pressure drops throughout the pump impeller as the cavitation increases.
- ❖ The sound pressure is increased due to propagation of cavitation at a particular speed of rotation and mass flow rate.
- ❖ The impeller blades are subjected to severe wall shear stress as the cavitation increases.

The findings of the present study will be useful for detecting the cavitation phenomenon through the sound produced by the pump impeller.

REFERENCES

Abdulaziz, A. M. and A. Kotb (2017). Detection of pump cavitation by vibration signature. *Australian Journal of Mechanical Engineering* 15(2), 103–110.

Al-hashmi, S. A. (2013). Statistical Analysis of Acoustic Signal for Cavitation Detection. *International Journal of Emerging Technology and Advanced Engineering* 3(4), 55–60.

ANSYS CFX-Solver Theory Guide. (2016), 15317(January), 362.

Banica, M. C., P. Limacher and H. Feld (2016). Analysis of the sources and the Modal content of the Acoustic field in a Radial Compressor outflow. In *Turbomachinery Technical Conference and Exposition* 1–14.

Barrio, R., E. Blanco, J. Keller, J. Parrondo and J. Fernandez (2011). Numerical determination of the acoustic impedance of a centrifugal pump. In *Joint Fluids Engineering Conference* 60, 1–8.

Binama, M., A. Muhirwa and E. Bisengimana (2016). Cavitation effects in centrifugal pumps-A review. *International Journal of Engineering Research and Applications (IJERA)* 6(5), 52–63.

Cunha, M. A. R. and H. F. V. Nova (2013). Cavitation modeling of a centrifugal pump

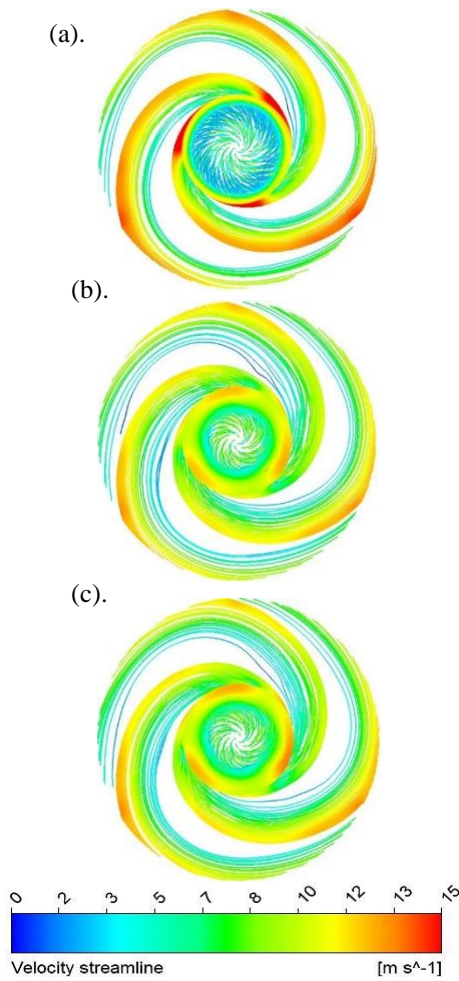


Fig. 11. Velocity streamline at (a). incipient cavitation (b). cavitation where efficiency is maximum and (c). super cavitation for mass flow rate at 40.17 kg/s.

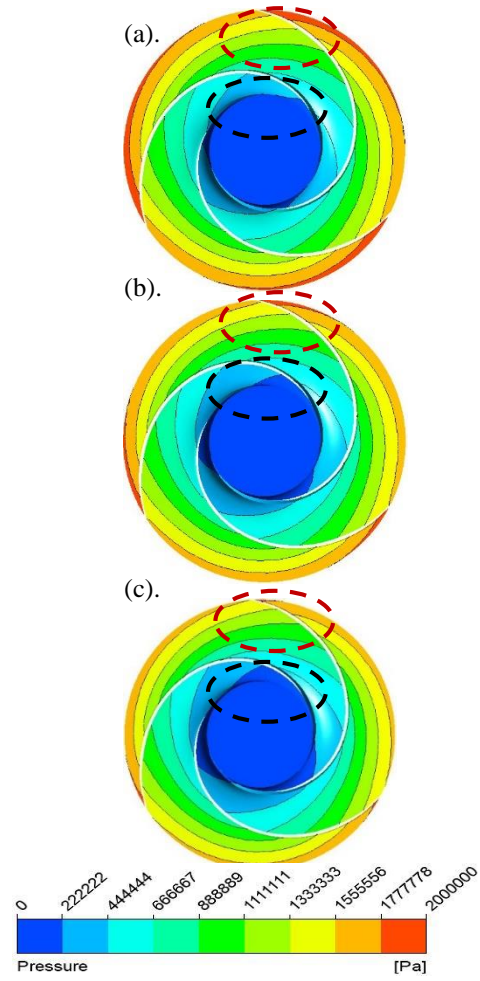


Fig. 12. Pressure contour at (a). incipient cavitation (b). cavitation where efficiency is maximum and (c). super cavitation for mass flow rate at 40.17 kg/s.

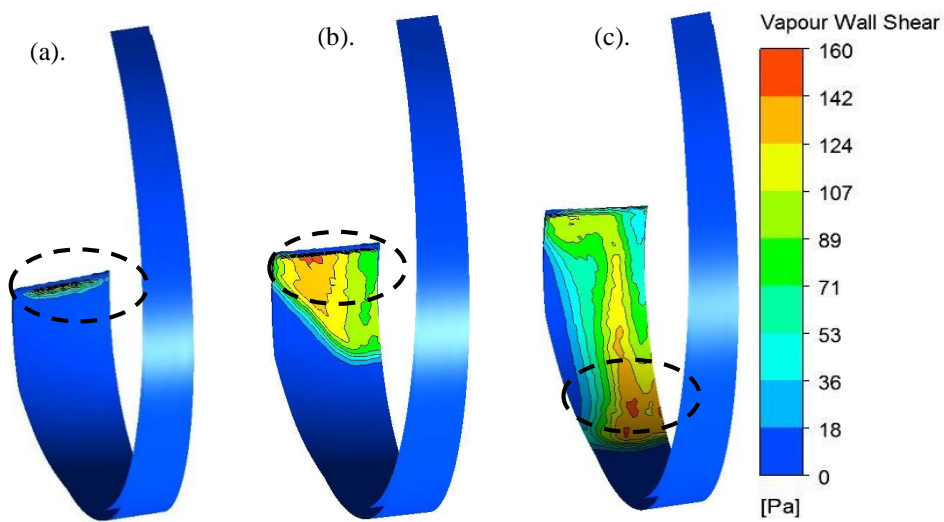


Fig. 13. Vapour shear stress contour at (a). incipient cavitation (b). cavitation where efficiency is maximum and (c). super cavitation for mass flow rate at 40.17 kg/s.

- impeller. In *22nd International Congress of Mechanical Engineering* 1633–1644.
- Dürer, B. and F. Wurm (2006). Noise sources in centrifugal pumps. In *2nd WSEAS Int. Conference on Applied and Theoretical Mechanics, Venice, Italy* 203–207.
- Ferrante, P., P. di. Francescantonio and P.-A. Hoffer (2014). Integrated “CFD-Acoustic” Computational Approach to the Simulation of Aircraft Fan Noise. In *Turbine Technical Conference and Exposition* 1–10.
- George, A. and D. P. Muthu (2016). CFD Analysis Of Performance Charectistics Of Centrifugal Pump Impeller To Minimising Cavitation. In *International Conference on Current Research in Engineering Science and Technology (ICCREST-2016)* 24–30.
- Iben, U. (2002). Modeling of cavitation. *Systems Analysis Modelling Simulation* 42(9), 1283–1307.
- Li, W. (2014). Validating full Cavitation model with an Experimental Centrifugal Pump. *Task Quarterly* 18(1), 81–100.
- Magagnato, F. and J. Zhang (2015). Simulation of a Centrifugal Pump by Using the Harmonic Balance Method. *International Journal of Rotating Machinery*.
- Maxime, B. and P. F. Chen-li (2015). Numerical Study and Analysis of Cavitation Performance in Centrifugal Impellers. *International Journal of Engineering Research and Technology (IJERT)* 4(09, September-2015), 552–556.
- Mckee, K. K., G. L. Forbes, I. Mazhar, R. Entwistle, M. Hodkiewicz and I. Howard (2015). A Vibration Cavitation Sensitivity Parameter Based On Spectral and Statistical Methods. *Elsevir* 42(January), 67–78.
- Michels, T., M. Markiewicz and Estorff, O. von. (2012). Sound Generation and Propagation in a Centrifugal Pump with the Finite Volume EIF-Approach. In *Turbo Expo 2012* (pp. 1–9).
- Mori, M., T. Masumoto, K. Ishihara, T. Oshima, Y. Yasuda and T. Sakuma (2014). Study on modeling of flow induced noise using Lighthill’s analogy and boundary element method. In *Inter-noise* 6–15.
- Muttalli, R. S., Agrawal, S., and Warudkar, H. (2014). CFD Simulation of Centrifugal Pump Impeller Using ANSYS-CFX. *International Journal of Innovative Research in Science, Engineering and Technology*, 3(8), 15553–15561.
- Pavesi, G., G. Ardizzon and G. Cavazzini (2005). Unsteady flow field and Noise generation in a Centrifugal Pump Impeller with a Vaneless Diffuser. In *Fluids Engineering Division Summer Meeting and Exhibition* 1–8.
- Pekker, M. and M. N. Shneider (2017). Initial stage of cavitation in liquids and its observation by Rayleigh scattering. *The Japan Society of Fluid Mechanics* 39(31 March), 13.
- Pode, M. V. P., P. S. V. Channapattana and P. A. A. Bagade (2015). Evaluating Performance of Centrifugal Pump through CFD while Modifying the Suction Side for Easting Discharge. *International Journal of Scientific and Research Publications* 5(3), 1–6.
- Pump Cavitation Causes* (2018). Retrieved from <http://www.enggcyclopedia.com/2011/11/pump-cavitation-causes/>
- Rehman, A. U., V. K. Kumar, A. R. Paul and A. Jain (2017). Performance and Cavitation Prediction in an Industrial Centrifugal Pump for Different Working Fluids. In *International Conference on Thermal and Fluid Engineering: ICTF-2017* (pp. 36–42).
- Rehman, A. U., A. Srivastava, A. Jain, A. R. Paul and R. Mishra (2015). Effect of Blade Trailing Edge Angle on the Performance of a Centrifugal Pump Impeller. In *28th International Congress of Condition Monitoring and Diagnostic Engineering* 702–706.
- Robinson, B. D. (2007). Acoustics Modeling in CFX. *The Focus* 60 (9 November-2007).
- Shi, L., D. Zhang, Y. Jin, W. Shi and Esch, B. P. M. (Bart) van. (2017). A study on tip leakage vortex dynamics and cavitation in axial- flow pump. *The Japan Society of Fluid Mechanics* 49, 19.
- Zhou, W., Z. Zhao, T. S. Lee and S. H. Winoto (2003). Investigation of Flow Through Centrifugal Pump Impellers Using Computational Fluid Dynamics. *International Journal of Rotating Machinery* 9(1), 49–61.